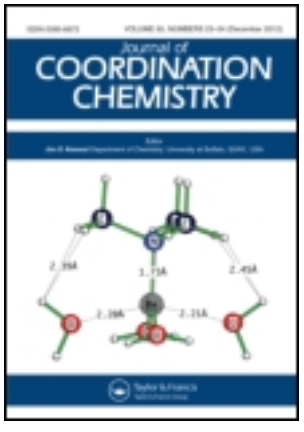


Journal of Coordination Chemistry
Publication details, including instructions for authors and subscription information:
http://www.tandfonline.com/loi/gcoo20

# New homo- and hetero-bimetallic assemblies based on 2,5-bis(4-carboxyphenylamino)-3,6-dichloro-1,4-benzoquinone: synthesis, characterization, and magnetic properties

Kumar Rakesh Ranjan [a] , Aparna Singh [a] , A. Banerjee [b] & B. Singh [a]

[a] Department of Chemistry, Faculty of Science , Banaras Hindu University , Varanasi-221005 , India

[b] UGC-DAE Consortium for Scientific Research, Khandwa Road , Indore-452017 , India

Published online: 15 Apr 2011.

To cite this article: Kumar Rakesh Ranjan , Aparna Singh , A. Banerjee & B. Singh (2011) New homo- and hetero-bimetallic assemblies based on 2,5-bis(4-carboxyphenylamino)-3,6-dichloro-1,4-benzoquinone: synthesis, characterization, and magnetic properties, Journal of Coordination Chemistry, 64:8, 1411-1425, DOI: 10.1080/00958972.2011.563382

To link to this article: http://dx.doi.org/10.1080/00958972.2011.563382

*Journal of Coordination Chemistry*
Vol. 64, No. 8, 20 April 2011, 1411–1425



# New homo- and hetero-bimetallic assemblies based on 2,5-bis(4-carboxyphenylamino)-3,6-dichloro-1,4-benzoquinone: synthesis, characterization, and magnetic properties

KUMAR RAKESH RANJAN†, APARNA SINGH†, A. BANERJEE‡ and B. SINGH*†

†Department of Chemistry, Faculty of Science, Banaras Hindu University, Varanasi-221005, India
‡UGC-DAE Consortium for Scientific Research, Khandwa Road, Indore-452017, India

(*Received 19 June 2010; in final form 10 January 2011*)

Synthesis, characterization, and magnetic properties of a new series of dinuclear compounds $M^{II}M'^{II}L_2(H_2O)_4$ (where $M^{II}$, $M'^{II}$ = Mn (**1**), Ni (**2**), Cu (**3**) and $M^{II}$ = Cu, $M'^{II}$ = Co (**4**), Ni (**5**); $LH_2$ = 2,5-bis(4-carboxyphenylamino)-3,6-dichloro-1,4-benzoquinone) are reported. These complexes were characterized by elemental analyses, FAB mass spectra, thermogravimetric analysis, spectroscopic techniques (infrared, NMR, UV-Vis), and powder XRD studies. Magnetic properties investigated by SQUID magnetometer show antiferromagnetic coupling between the metal centers connected by the extensive $\pi$-delocalized ligand. Magnetic coupling constants ($J$) ranging from $-1.01$ to $-3.01\,cm^{-1}$ based on the Hamiltonian $H = -2JS_iS_j$ have been obtained. The optimized geometry of the ligand derived from DFT is also reported.

*Keywords*: Bimetallic assemblies; Bicarboxylate ligand; SQUID; Magnetic properties; $\pi$-Delocalized; Coupling constant; DFT



## 1. Introduction

Coordination chemistry has given attention to the design and synthesis of molecular magnetic materials because of their applications as catalytic, luminescent, magnetic, porous, conductive, chiral, or non-linear optical materials [1–4]. The chemistry of coordination polymers containing paramagnetic metal ions and exhibiting fascinating extended structures are of importance due to their potential applications in molecular magnetism [3–9]. Considerable work has been dedicated to the properties of homo/hetero polynuclear 3d-metal complexes, which are valuable models for biological systems and molecular functional materials in magnetism [10, 11], optics [12, 13], electronics [14], molecular adsorption, light conversion devices, and bimetallic catalysis [15, 16]. The first step in preparation of molecular magnets is the synthesis and characterization of bridging ligands [17–20] because these molecules can bridge metal

*Corresponding author. Email: bsinghbhu@rediffmail.com

*Journal of Coordination Chemistry*
ISSN 0095-8972 print/ISSN 1029-0389 online 
DOI: 10.1080/00958972.2011.563382

ions, opening a way to extended magnetic structures. A good bridging ligand can effectively and efficiently transmit the magnetic coupling between paramagnetic centers. The bridging ligands like cyanide [21–25], dicyanamide [26], oxalate [27], azide [28–31], and carboxylate [32] have been widely investigated and numerous compounds have been reported. The design and synthesis of new metal organic frameworks have received considerable interest owing to their potential applications [33, 34] as functional materials in molecular magnetism. The molecular magnet is generated by the combination of d/f block metal ions with polydentate ligands [35, 36]. The structure and properties of such materials depend on (a) reaction condition, (b) coordination ability of the ligand, (c) metal ion coordination geometry, (d) metal ligand ratio [35, 37–41], etc. The various modes of bonding [42] of carboxylates have been used to construct dimensionally extended metal complexes. Benzoquinones are interesting systems for electron transfer reactions, which play an important role in biological systems [43–46]. Hendrickson *et al*. [47] studied magnetic coupling in dinuclear copper(II) compounds with internuclear separation in excess of 12 Å. The magnetic exchange *via* bridging ligands with extensive $\pi$-delocalization was better than with saturated carbons. To study the magnetic exchange *via* $\pi$-delocalized ligands, synthesis, structure, and magnetic studies of homo- and hetero-bimetallic (3d) complexes of 2, 5-bis(4-carboxyphenylamino)-3,6-dichloro-1,4-benzoquinone are undertaken. In this article studies on bimetallic complexes of 2,5-bis(4-carboxyphenylamino)-3,6-dichloro-1, 4-benzoquinone are reported.

## 2. Experimental materials

### 2.1. *Physical measurements and materials*

4-Aminobenzoic acid (Aldrich, USA), *p*-chloranil (2,3,5,6-tetrachloro-1,4-benzoquinone; Himedia, India), hydrated metal chlorides $MnCl_2 \cdot 4H_2O$ (Merck, India), $CoCl_2 \cdot 6H_2O$ (BDH, India), $NiCl_2 \cdot 6H_2O$ (s.d. fine chem., India), and $CuCl_2 \cdot 2H_2O$ (Merck, India) were used as obtained. Elemental analyses were performed on a CE-440 Exeter Analytical CHN analyzer. Infrared (IR) spectra were recorded on a Varian 300 FT-IR Excalibur spectrophotometer from 4000 to 400 $cm^{-1}$ (KBr) and from 400 to 100 $cm^{-1}$ (Nujol film). $^1H$ and $^{13}C$ NMR spectra in DMSO-$d_6$ were obtained on a JEOL FT NMR AL 300 MHz spectrometer using tetramethylsilane (TMS) as the internal standard. FAB-mass spectra (FAB-MS) were recorded on a Jeol SX 102/Da-600 mass spectrometer/data system using Argon/Xenon (6 kv, 10 mA as the FAB gas). Solid state UV-Vis spectra were obtained on a UV-1700 Pharma spec. Shimadzu UV spectrophotometer in Nujol mulls. X-ray diffraction (XRD) pattern was obtained on an ID 3000 Rich Scifert X-Ray diffraction system using Cu-K$\alpha$ ($\lambda = 1.540598$ Å) radiation. Thermogravimetric analysis (TGA) thermograms were recorded on Diamond TG/DTA Perkin Elmer equipment. Variable temperature DC magnetic susceptibilities of polycrystalline samples were measured on a Quantum Design, MPMS-XL magnetometer in a field of 1 T from 2 to 300 K. The data were corrected for experimentally determined contribution of the sample holder. Magnetization *versus* field measurement was performed with a PPMS-14 T (Quantum Design, USA) magnetometer. Corrections for the diamagnetic response of the compounds due to closed atomic shells as estimated

from Pascal's constants [48] were applied. The program JulX [49] was used for simulation and analysis of magnetic susceptibility data. JulX calculates magnetic properties by using the spin Hamiltonian $H = -2JS_iS_j$ (where i and j make reference to the different paramagnetic centers) to describe the interactions between the two paramagnetic centers present in bimetallic complexes.

## 2.2. *Synthesis of the complexes*

**2.2.1. Synthesis of 2,5-bis(4-carboxyphenylamino)-3,6-dichloro-1,4-benzoquinone ($LH_2$).** In a suspension of *p*-chloranil (0.246 g, 1 mmol) in ethanol (10 mL), 4-aminobenzoic acid (0.274 g, 2 mmol) was added. The resulting mixture was stirred for 8 h at room temperature. A dark brown precipitate was obtained which was filtered and washed with acetone (4–5 times) to remove any trace of the unreacted reagent. The vacuum-dried compound (brown, 68% based on *p*-chloranil, decomposing at ~286°C) was further characterized. The calculated values of vibration frequencies are within the brackets. Anal. Calcd for $C_{20}H_{12}N_2O_6Cl_2$ (%): C, 53.71; H, 2.70; N, 6.26. Found (%): C, 53.75; H, 2.62; N, 6.20. $^1$H NMR (DMSO, TMS) $\delta_H$ (ppm): 12.792 (s, 2 H, acidic), 9.774 (s, 2 H, NH), 7.891–7.873 (d, 4 H, ArH), 7.207–7.187 (d, 4 H, ArH ). $^{13}$C NMR, $\delta_C$ (ppm): 174.465 (s, 2 C, C=O quinonic), 166.924 (s, 2 C, C=O acidic), 142.356–142.100 (d, 4 C, C–N), 129.276, 126.103, 123.012, 122.081 (aromatic), 108.870 (s, 2 C, C–Cl). FAB-MS (*m*/*z*): 447 ($M^+$). UV-Vis (nujol; $\lambda_{max}$, $cm^{-1}$): 25,706, 29,850, 34,013, and 42,553. FT-IR ($cm^{-1}$): $\nu$(N–H) 3447 s [3473], $\nu$(C–H) 3261w [3212], $\nu$(C=$O_{quinone}$) 1665 m [1700], $\nu$(C–C) 1589 s [1607], $\rho$(N–H) + $\nu$(C=$C_{quinonic}$) 1496 s [1489], $\nu$(C–N) 1419w [1383], $\alpha_{quinone}$ + $\nu$(C–N) 1292 s [1289], $\nu$(C–C) + $\nu$(C–N) 1251w [1249], $\rho$(C–H) + $\rho$(O–H) 1174 s [1184], $\nu_{ring}$ + $\nu$(C–O) 1113 s [1101], $\alpha$ 1011w [1018], $\nu$(C–Cl) 896w [901], $\omega$(C–H) 859w [850], $\Phi + \delta_{ring}$ 759w [754], $\Phi$ 701w [705], $\omega$(N–H) 609w [609], $\omega$(O–H) 496w [488].

**2.2.2. Synthesis of $Mn_2^{II}L_2(H_2O)_4$ (1).** $LH_2$ (0.894 g, 2 mmol) was dissolved in water (15 mL) by adding KOH (0.224 g, 4 mmol, 3 mL) solution. To the resulting dark brown solution an aqueous solution of hydrated Mn(II) chloride (0.395 g, 2 mmol) was added dropwise. A microcrystalline precipitate started to appear after a few minutes. The complex thus obtained was filtered off, washed repeatedly with water and water/ethanol (1 : 1, v/v) mixture, and then dried under reduced pressure (brown, 53% based on ligand, decomposes at ~293°C). Anal. Calcd for $Mn_2C_{40}H_{28}N_4O_{16}Cl_4$ (%): C, 44.80; H, 2.63; N, 5.22. Found (%): C, 44.88; H, 2.56; N, 5.15. FT-IR ($cm^{-1}$): $\nu$(N–H) + $\nu$(O–$H_w$) 3397 m, $\nu$(C–H) 3232w, $\nu$(C=$O_{quinone}$) 1655 m, $\nu_{as}(CO_2^-)$ 1572 s, $\nu_s(CO_2^-)$ 1482 m, $\nu$(C–N) 1401w, $\alpha_{quinone}$ + $\nu$(C–N) 1298w, $\rho$(C–H) + $\rho$(O–H) 1187w, $\nu_{ring}$ + $\nu$(C–O) 1106w, $\alpha$ 1016 m, $\nu$(C–Cl) + $\rho(H_2O)$ 894 m, $\Phi$ + $\nu$(Mn–OH) 706w, $\rho(H_2O)$ 557 m, $\pi$(Mn–OH) 456w, $\nu$(Mn–O) 325w, 145w $\rho$(C–Cl) + $\delta$(Mn–OH).

The $Ni_2^{II}$ (**2**) and $Cu_2^{II}$ (**3**) analogs were prepared by using similar procedure.

**2.2.3. $Ni_2^{II}L_2(H_2O)_4$ (2) (black, 50% based on ligand, decomposes at ~300°C).** Anal. Calcd for $Ni_2C_{40}H_{28}N_4O_{16}Cl_4$ (%): C, 44.49; H, 2.61; N, 5.21. Found (%): C, 44.56; H, 2.66; N, 5.15. FAB-MS (*m*/*z*): 1078 ($M^+$). UV-Vis (nujol; $\lambda_{max}$, $cm^{-1}$): 10,256, 14,285, 25,725, 29,775, 34,150, and 42,550. FT-IR ($cm^{-1}$): $\nu$(N–H) + $\nu$(O–$H_w$) 3373 m, $\nu$(C–H)

3219w, $\nu$(C=$O_{quinone}$) 1662 m, $\nu_{as}(CO_2^-)$ 1582 s, $\nu_s(CO_2^-)$ 1482 m, $\nu$(C–N) 1395 m, $\alpha_{quinone} + \nu$(C–N) 1292 m, $\rho$(C–H) + $\rho$(O–H) 1170w, $\nu_{ring} + \nu$(C–O) 1104w, $\alpha$ 1016w, $\nu$(C–Cl) + $\rho(H_2O)$ 894 m, $\Phi$ 697w, $\nu$(Ni–OH) + $\rho(H_2O)$ 556w, $\pi$(Ni–OH) 355w, $\nu$(Ni–O) 290w, $\rho$(C–Cl) + $\delta$(Ni–OH) 153w.

**2.2.4. $Cu_2^{II}L_2(H_2O)_4$ (3) (black, 58% based on ligand, decomposes at ~295°C).** Anal. Calcd for $Cu_2C_{40}H_{28}N_4O_{16}Cl_4$ (%): C, 44.09; H, 2.59; N, 5.14. Found (%): C, 44.17; H, 2.67; N, 5.06. UV-Vis (nujol; $\lambda_{max}$, $cm^{-1}$): 15,455, 25,715, 29,870, 34,000, and 42,546. FT-IR ($cm^{-1}$): $\nu$(N–H) + $\nu$(O–H) 3451 m, $\nu$(C–H) 3257w, $\nu$(C=$O_{quinone}$) 1666 m, $\nu_{as}(CO_2^-)$ 1595 s, $\nu_s(CO_2^-)$ 1482 s, $\nu$(C–N) 1401w, $\alpha_{quinone} + \nu$(C–N) 1285 s, $\rho$(C–H) + $\rho$(O–H) 1169w, $\nu_{ring} + \nu$(C–O) 1105w, $\alpha$ 1012w, $\nu$(C–Cl) + $\rho(H_2O)$ 899w, $\Phi$ 713w, $\nu$(Cu–O) + $\rho(H_2O)$ 526w, $\nu$(Cu–O) 385w, $\rho$(C–Cl) + $\delta$(Cu–OH) 158w.

**2.2.5. Synthesis of $Cu^{II}Co^{II}L_2(H_2O)_4$ (4).** An aqueous solution (3 mL) containing hydrated Cu(II) chloride (0.170 g, 1 mmol) and hydrated Co(II) chloride (0.237 g, 1 mmol) was added dropwise to ligand solution prepared as above. A microcrystalline precipitate started to appear after a few minutes. The complex thus precipitated was filtered off, washed repeatedly with water and water/ethanol (1 : 1, v/v), and then dried under reduced pressure (black, 72% based on ligand, decomposing at ~285°C). Anal. Calcd for $CuCoC_{40}H_{28}N_4O_{16}Cl_4$ (%): C, 44.28; H, 2.60; N, 5.16. Found (%): C, 44.35; H, 2.69; N, 5.12. FAB-MS ($m/z$): 1085 ($M^+$). UV-Vis (nujol; $\lambda_{max}$, $cm^{-1}$): 9852, 18,315, 25,735, 29,859, 34,106, and 42,525. FT-IR ($cm^{-1}$): $\nu$(N–H) + $\nu$(O–$H_w$) 3377 m, $\nu$(C–H) 3258w, $\nu$(C=$O_{quinone}$) 1665 m, $\nu_{as}(CO_2^-)$ 1593 s, $\nu_s(CO_2^-)$ 1485 s, $\nu$(C–N) 1372 m, $\alpha_{quinone} + \nu$(C–N) 1284w, $\rho$(C–H) + $\rho$(O–H) 1168w, $\nu_{ring} + \nu$(C–O) 1104w, $\alpha$ 1013w, $\nu$(C–Cl) + $\rho(H_2O)$ 899 m, $\pi_{ring} + \delta$(Cu–OH) 713w, $\nu$(Co–O) + $\rho(H_2O)$ 548w, $\delta$(Cu–OH) + $\pi$(Co–OH) 489w, $\nu$(Cu–OH) 385w, $\nu$(Co–OH) 326w, $\rho$(C–Cl) + $\delta$(Co–OH) 150w.

The $Cu^{II}Ni^{II}$ (**5**) analog was prepared following the above procedure.

**2.2.6. $Cu^{II}Ni^{II}L_2(H_2O)_4$ (5) (black, 58% based on ligand, decomposes at ~305°C).** Anal. Calcd for $CuNiC_{40}H_{28}N_4O_{16}Cl_4$ (%): C, 44.29; H, 2.60; N, 5.19. Found (%): C, 44.37; H, 2.68; N, 5.14. UV-Vis (nujol; $\lambda_{max}$, $cm^{-1}$): 10,504, 14,245, 25,775, 29,790, 34,006, and 42,678. FT-IR ($cm^{-1}$): $\nu$(N–H) + $\nu$(O–$H_w$) 3399 m, $\nu$(C–H) 3257w, $\nu$(C=$O_{quinone}$) 1660 s, $\nu_{as}(CO_2^-)$ 1594 s, $\nu_s(CO_2^-)$ 1493 m, $\nu$(C–N) 1378 m, $\alpha_{quinone} + \nu$(C–N) 1284 m, $\rho$(C–H) + $\rho$(O–H) 1168 m, $\nu_{ring} + \nu$(C–O) 1103w, $\alpha$ 1013w, $\nu$(C–Cl) + $\rho(H_2O)$ 900w, $\pi_{ring} + \delta$(Cu–OH) 713w, $\nu$(Ni–OH) + $\rho(H_2O)$ 534w, $\delta$(Cu–OH) 486w, $\nu$(Cu–OH) 398w, $\pi$(Ni–OH) 359w, $\nu$(Ni–O) 289w, $\rho$(C–Cl) + $\delta$(Cu–OH) 153w.

### 2.3. *Computational details*

The optimized geometry of 2,5-bis(4-carboxyphenylamino)-3,6-dichloro-1,4-benzoquinone was obtained by RHF/6-31 + G*, B3LYP/6-31 + G*, and B3LYP/6-311 + +G** methods [50]. Calculations of structural parameters, atomic charges, and vibrational frequencies (with intensity) of the ligand were carried out by Gaussian 03 [51]. The calculated values of vibrational frequencies vary by 4.5% from the experimental values,

with the expected range of agreement for B3LYP density functional theory [52]. The experimentally observed vibrational frequencies are assigned with the help of G view.

## 3. Results and discussion

The compound 2,5-bis(4-carboxyphenylamino)-3,6-dichloro-1,4-benzoquinone ($LH_2$; figure 1) and its homo- and hetero-bimetallic complexes (**1–5**) have been prepared; elemental data confirm the formation of the compounds. The complexes are insoluble in common organic solvents such as chloroform, carbon tetrachloride, methanol, ethanol, and DMF, but are slightly soluble in DMSO and hot water.

### 3.1. *IR spectral studies*

Absorption bands of the ligand are assigned with the help of vibrational output of Gaussian (Supplementary material, table S1). Bands at 4000–2600 $cm^{-1}$ comprise stretching frequencies due to –OH, –NH, and C–H groups. Bands at 1665, 1589, 1496, 1292, and 896 $cm^{-1}$ are attributed to $\nu(C{=}O_{quinone})$, $\nu(C{-}C)$, $\rho(N{-}H) + \nu(C{=}C_{quinonic})$, $\alpha_{quinone} + \nu(C{-}N)$, and $\nu(C{-}Cl)$, respectively. The carboxylate may be bonded to a metal unidentate, chelating, and bridging bidentate [53]. The magnitude of difference ($\Delta\nu$) between the $\nu_{as}(CO_2^-)$ and $\nu_s(CO_2^-)$ in spectra of **1–5** is used for distinction among the three modes of bonding. The value of $\Delta\nu(CO_2^-)$ lying in the range 90–113 suggests bidentate chelating bonding of the carboxylate ion [53]. Far IR spectra of the metal complexes exhibit major bands at 390, 360, and 150, which are assigned to $\nu(M{-}O)$, $\pi(M{-}OH_w)$, and $\rho(C{-}Cl) + \delta(M{-}OH_w)$, respectively.

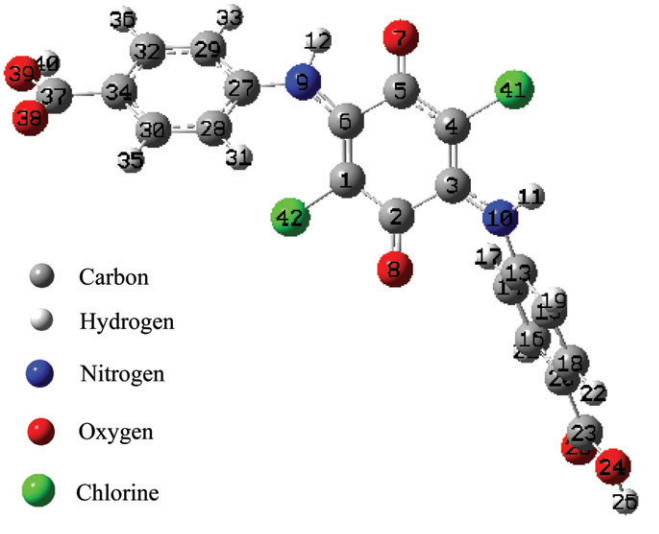


Figure 1. Optimized molecular structure of $LH_2$ (numbering is not as per IUPAC nomenclature).

### 3.2. *Mass spectral (FAB-MS) studies*

FAB-MS (Supplementary material, figure S1) of the ligand, **2** and **4** exhibit molecular ion peaks at $m/z$ 447, 1078, and 1085, respectively. Chlorine has two isotopes: $^{35}$Cl (75.8%) : $^{37}$Cl (24.2%) (3 : 1); the peak in the spectrum of ligand at $m/z$ 447 corresponds to the molecular weight of ligand based on $^{35}$Cl. The peak at $m/z$ 451 corresponds to the isotopic peak for $^{37}$Cl [54]. The intensity of the peaks at $m/z$ 447 and 451 is almost in the ratio of 3 : 1. Molecular ion peaks in the spectra of the metal complexes correspond to molecular weights of the complexes based on the atomic weights of $^{58}$Ni (**2**), $^{63}$Cu, and $^{59}$Co (**4**) isotopes; among several molecular weights based on the isotope distribution of the metal [55]. Molecular ion peaks of complexes have been used to confirm the proposed formula. There are many peaks between $m/z$ 1078 and 1082 because of various combinations of Cl and Ni isotopes. The spectrum also showed isotope cluster peaks at $m/z$ 1006 and 1008, at 562 and 564, at 504 and 506, corresponding to the molecular weights of the complex cations $[Ni_2L_2]^+$ (loss of four coordinated water molecules), $[Ni_2L]^+$, and $[NiL]^+$, respectively. In the spectrum of CuCo complex the isotopic patterns are clearly observed: 1085 ($[M]^+$, $^{63}$Cu); 1087 ($[M+2]^+$, $^{65}$Cu). The fragments of the ligand and complexes produced are given in Supplementary material, table S2.

### 3.3. *NMR spectral studies*

$^1$H and $^{13}$C NMR signals of the ligand are assigned with the help of Mulliken charge on a particular atom. $^1$H NMR spectra (Supplementary material, figure S2a) display peaks at 12.79, 9.77, 7.89, 7.87, 7.21, and 7.19, which are attributed to the pairs ($H^{26}$,$H^{40}$); ($H^{11}$,$H^{12}$); ($H^{22}$,$H^{36}$); ($H^{21}$,$H^{35}$); ($H^{17}$,$H^{33}$); and ($H^{19}$,$H^{31}$), respectively. The $^{13}$C NMR spectrum (Supplementary material, figure S2b) displays peaks at 174, 167, 142, 142, 129, 126, 123, 122, and 109, which are assigned to the pairs ($C^2$,$C^5$); ($C^{23}$,$C^{37}$); ($C^{13}$,$C^{27}$); ($C^3$,$C^6$); ($C^{20}$,$C^{34}$); ($C^{16}$,$C^{18}$,$C^{30}$,$C^{32}$); ($C^{14}$,$C^{28}$); ($C^{15}$,$C^{29}$); and ($C^1$,$C^4$), respectively.

### 3.4. *UV-Vis spectral studies*

Absorption bands at 25,125, 26,315, 29,673, 34,723, and 41,667 cm$^{-1}$ observed in the spectrum of *p*-chloranil are assigned to $n$–$\pi^*$ and $\pi$–$\pi^*$ transitions. These transitions are observed at 25,706, 29,850, 34,013, and 42,553 cm$^{-1}$ in the spectrum of 2,5-bis(4-carboxyphenylamino)-3,6-dichloro-1,4-benzoquinone. Two new bands at 10,256 and 14,285 cm$^{-1}$ in the spectrum of the $Ni_2$ complex, attributed to $^3A_{2g}(F) \rightarrow {}^3T_{2g}(F)$ and $^3A_{2g}(F) \rightarrow {}^3T_{1g}(F)$ transitions, respectively, show octahedral $Ni^{II}$. One absorption at 15,455 cm$^{-1}$ in the spectrum of $Cu_2$ complex is assigned to $^2E_g \rightarrow {}^2T_{2g}(D)$ transition for octahedral $Cu^{II}$. The spectrum of CuCo complex exhibits bands at 9852 and 18,315 cm$^{-1}$, assigned to $^4T_{1g}(F) \rightarrow {}^4T_{2g}(F)$ and $^4T_{1g}(F) \rightarrow {}^4T_{1g}(P)$ transitions of $Co^{II}$, respectively, and a band at 14,430 cm$^{-1}$ is attributed to $^2E_g \rightarrow {}^2T_{2g}(D)$ of $Cu^{II}$. In the spectrum of CuNi complex two bands appear at 10,504 and 14,245 cm$^{-1}$, the first one is assigned to $^3A_{2g}(F) \rightarrow {}^3T_{2g}(F)$ transition of $Ni^{II}$ and another one is assigned to $^2E_g \rightarrow {}^2T_{2g}(D)$ transition of $Cu^{II}$. These spectral features are characteristic of an octahedral coordination around the metal ions.

### 3.5. *Thermal analysis*

TGA of $Mn_2$, $Cu_2$, and CuNi were carried out by heating at $10^{\circ}C\,min^{-1}$ the samples in oxygen from 25°C to 800°C to study their robustness and decomposition pathways. The thermograms show weight loss mainly in two steps. Compound $Mn_2$ (figure 2a) undergoes weight loss of ~ 12.62% at 129°C due to ejection of four waters and two $CO_2$ molecules (Calcd ~14.92%). Further decomposition continues to 435°C, and the residue of 17.81% at 800°C corresponds to MnO (Calcd ~13.23%). A loss of ~16.31% occurs for the $Cu_2$ compound from 50°C to 273°C (figure 2b), corresponding to loss of four waters and two $CO_2$ molecules (Calcd ~14.69%). On further heating, weight loss occurs from 273°C to 447°C due to combustion of the organic components. The residue ~18.0% at 800°C corresponds to the formation of CuO (Calcd ~14.6%). For the CuNi compound (figure 2c) the weight loss (~20.36%) occurs at 211°C, which corresponds to loss of four water molecules and three $CO_2$ molecules (Calcd ~18.81%). Further heating causes decrease in weight of ~14.10% in the temperature range 211–327°C due to the escape of one $CO_2$ and two $Cl_2$ molecules (Calcd ~17.13%). The decomposition of the residue starts at 327°C showing loss of ~44.37% between 327°C and 426°C, followed by a further loss of ~7.51% up to 800°C. The residue (~13.65%) corresponds to the formation of CuO + NiO (~14.21%, Calcd).

### 3.6. *Powder XRD studies*

Powder XRD diffractograms of the ligand and the $Ni_2$ complex are shown in Supplementary material figures S3a and S3b, respectively. The observed diffraction data such as d-values, relative intensities, and $2\theta$ are given in Supplementary material tables S3a, S3b, and S3c. Ito's method [56] of indexing of the pattern indicated triclinic primitive lattice structure for the ligand and for the $Ni_2$ and CuCo complexes, with the cell parameters for $LH_2$: $a = 13.6124 \pm 0.0311$ Å, $b = 10.6883 \pm 0.0115$ Å, $c = 11.6057 \pm 0.0163$ Å, $\alpha = 83.87 \pm 0.09^{\circ}$, $\beta = 88.99 \pm 0.12^{\circ}$ and $\gamma = 86.06 \pm 0.11^{\circ}$; for $Ni_2$: $a = 12.8634 \pm 0.0212$ Å, $b = 10.3538 \pm 0.0132$ Å, $c = 8.8936 \pm 0.0126$ Å, $\alpha = 73.23 \pm 0.12^{\circ}$, $\beta = 89.06 \pm 0.17^{\circ}$, and $\gamma = 86.07 \pm 0.13^{\circ}$; for CuCo: $a = 12.7017 \pm 0.1431$ Å, $b = 10.4013 \pm 0.0929$ Å, $c = 8.7491 \pm 0.0616$ Å, $\alpha = 73.65 \pm 0.47^{\circ}$, $\beta = 90.72 \pm 0.41^{\circ}$, and $\gamma = 86.68 \pm 0.71^{\circ}$. Both $Ni_2$ and CuCo complexes have almost similar lattice parameters. Using these unit cell parameters, calculated diffraction data and indices of $LH_2$ and of both the complexes are included in Supplementary material tables S3a, S3b, and S3c. Because of the presence of carboxy groups at both ends of ligand, the ligand and complexes have 1-D structure along the *c*-axis but in the ligand it is due to the hydrogen bonding (Supplementary material, figure S3c) and in the metal complexes it is due to coordination between the metal and the ligand. The stronger metal bonding in the complexes results in contraction of the unit cell along the *c*-axis compared to the ligand. Thus, the ligand and the complexes are isomorphic and 1-D along the *c*-axis.

### 3.7. *Direct current magnetic susceptibility and magnetization studies*

**Complex 1.** Solid-state variable temperature magnetic susceptibility measurements were carried out on microcrystalline samples from 2 to 300 K. The temperature variation of $\chi_M T$ is shown in figure 3. The value of $\chi_M T$ at 300 K is 7.51 $cm^3\,mol^{-1}\,K$ (7.75 $\mu_B$) per

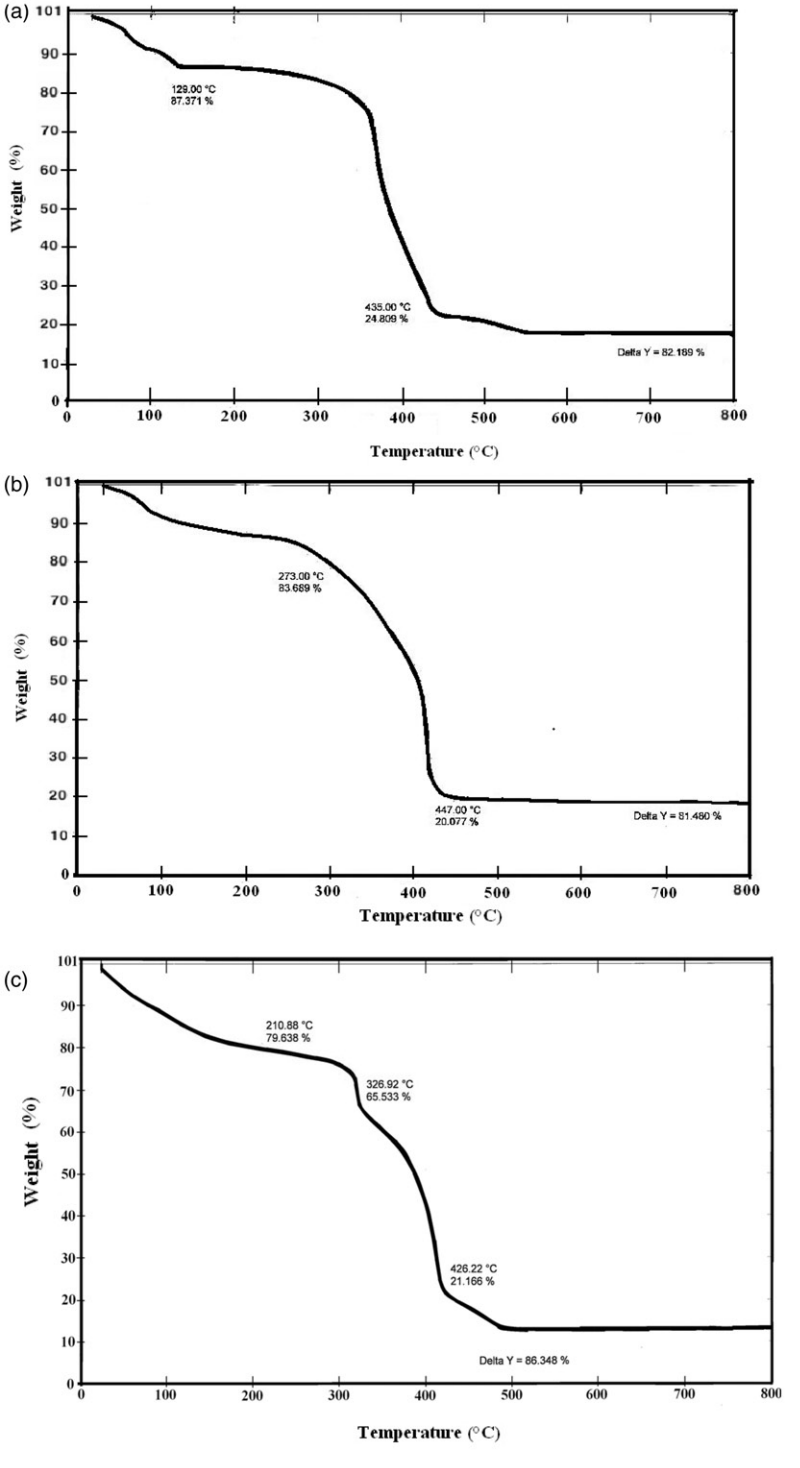


Figure 2. TGA thermograms of (a) Compound $Mn_2$, (b) Compound $Cu_2$, and (c) Compound CuNi.

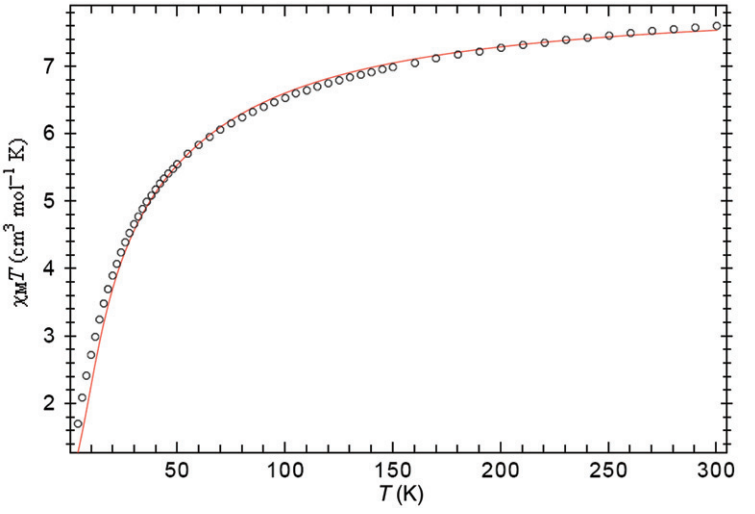


Figure 3. $\chi_M T$ *vs.* $T$ plot for **1** at 1 T: circle (experimental) and red line (calculated) with the parameters reported in the text.

two $Mn^{II}$ ions, much lower than the spin-only value 8.85 $cm^3 mol^{-1} K$ (8.41 $\mu_B$) expected for two uncoupled $Mn^{II}$ ions ($S = 5/2$, $g = 2$). This suggests antiferromagnetic interactions between the metal ions at room temperature. The $\chi_M T$ decreases slowly on lowering the temperature to 70 K giving a value 6.04 $cm^3 mol^{-1} K$ (6.95 $\mu_B$), followed by a rapid decrease attaining value 1.18 $cm^3 mol^{-1} K$ (3.07 $\mu_B$) at 2 K. The $\chi_M T$ at 2 K is close to the value for $S = 1$ (2.83 $\mu_B$); such magnetic behavior is typical for antiferromagnetic coupling between $Mn^{II}$ ions in the chain. The magnetic susceptibility of the polycrystalline sample obeys the Curie–Weiss law [$\chi = C/(T - \theta)$] between 12 and 300 K. The best linear fit of $\chi_M^{-1}$ *versus* $T$ (Supplementary material, figure S4a) data with the Curie–Weiss law gives the Curie constant $C = 8.03\ cm^3 K mol^{-1}$. The Curie constant $C$ is used to calculate $\mu_{eff}$ [$\mu_{eff} = (8\,C)^{1/2}$] [57]. The resulting $\mu_{eff}$ (from $C$) = 8.01 $\mu_B$ is very close to the experimental value of 7.75 $\mu_B$, and is in accord with a high spin ($S = 5/2$) $Mn^{II}$. To investigate the magnitude of the magnetic interaction between $Mn^{II}$ and $Mn^{II}$ ions, a satisfactory fit of the data was obtained with $J_{12} = -1.44\ cm^{-1}$, $g_{Mn} = 1.994$, TIP = $7 \times 10^{-6}\ cm^3 mol^{-1}$ [58], $\theta = -0.41$ K, and PI = 0.80%. The plot of $M/N\beta$ *versus* $H$ (figure 4) at 5 K indicates that the magnetization at 14 T achieves only 6.06 $N\beta$ instead of 9.97 $N\beta$, expected for two $Mn^{II}$ ($S = 5$, $g_{eff} = 1.994$) ions. The field dependence of the magnetization ($M$) at 5.0 K exhibits a continuous increase with the magnetic field and neither saturation nor hysteresis loop is observed. Most likely, the lack of saturation of the magnetization at this temperature is due to the magnetic field overcoming weak intrachain antiferromagnetic interactions.

The magnetic susceptibility results for polycrystalline **2**, **3**, **4**, and **5** obey the Curie–Weiss law from 16 to 300, 13 to 300, 36 to 300, and 70 to 300 K, respectively. The best fit values of the Curie ($C$) constants are 2.15, 1.21, 2.98, and 2.32 $cm^3 K mol^{-1}$, respectively. The $\mu_{eff}$ values calculated from $C$ are 4.15, 3.11, 4.88, and 4.31 $\mu_B$, respectively, in good agreement with the experimental values of 4.09, 2.97, 4.65, and 4.07 $\mu_B$, respectively. The plots of $\chi_M^{-1}$ *versus* $T$ are shown in Supplementary material, figure S4.

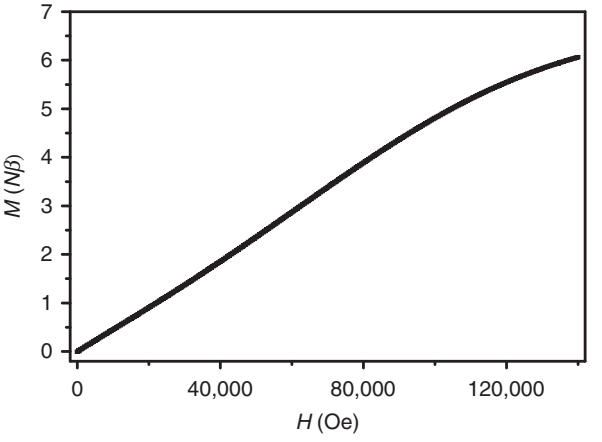


Figure 4. Magnetization *vs.* field (Oe) measurements for **1** (at 5 K).

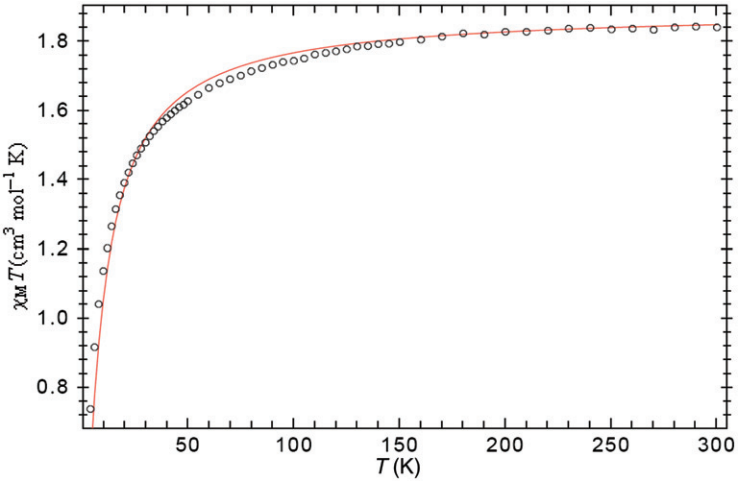


Figure 5. $\chi_M T$ *vs.* $T$ plot for **2** at 1 T: circle (experimental) and red line (calculated) with the parameters reported in the text.

**Complex 2.** At room temperature, $\chi_M$T (figure 5) has a value of 2.09 $cm^3\,mol^{-1}$ K (4.09 $\mu_B$), slightly higher than the spin-only value of 1.99 $cm^3\,mol^{-1}$ K (3.99 $\mu_B$) expected for two uncoupled octahedral $Ni^{II}$ ions ($S=1$, $g=2$), which may be attributed to the spin-orbital coupling of the $Ni^{II}$ ion. With a decrease in temperature, $\chi_M T$ decreases gradually, reaching a minimum of 0.50 $cm^3\,mol^{-1}$ K (2.01 $\mu_B$) [$\mu_{eff}=2.828(\chi_M^{corr}T)^{1/2}$ (B.M.)] at 2 K, indicating antiferromagnetic coupling between the $Ni^{II}$ ions. To investigate the magnitude of the magnetic interaction between $Ni^{II}$ and $Ni^{II}$ ions, a fit of the data was made using a model for a chain of $Ni^{II}$. A satisfactory fit was obtained with $J_{12}=-1.01\,cm^{-1}$, $g_{Ni}=2.016$, TIP $=5\times10^{-6}\,cm^3\,mol^{-1}$ [59], $\theta=-0.16$ K, and PI $=0.46\%$, showing antiferromagnetic behavior of the system. The magnetic susceptibility, $\chi_M$ (Supplementary material, figure S5), shows a steady increase upon cooling,

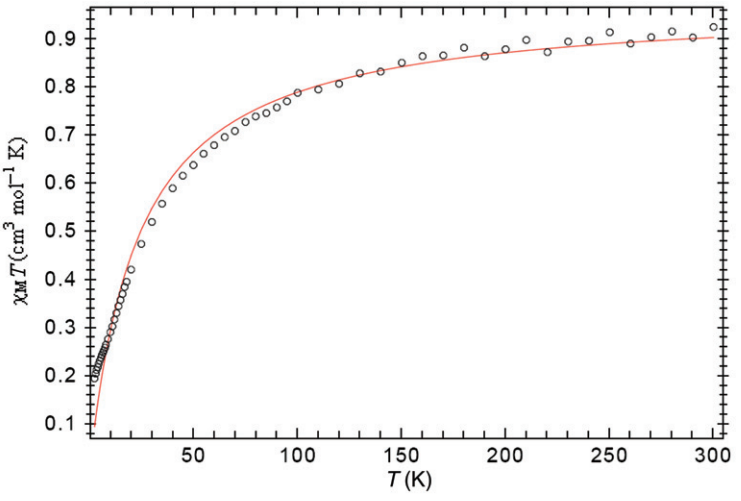


Figure 6. $\chi_M T$ *vs.* $T$ plot for **3** at 1 T: circle (experimental) and red line (calculated) with the parameters reported in the text.

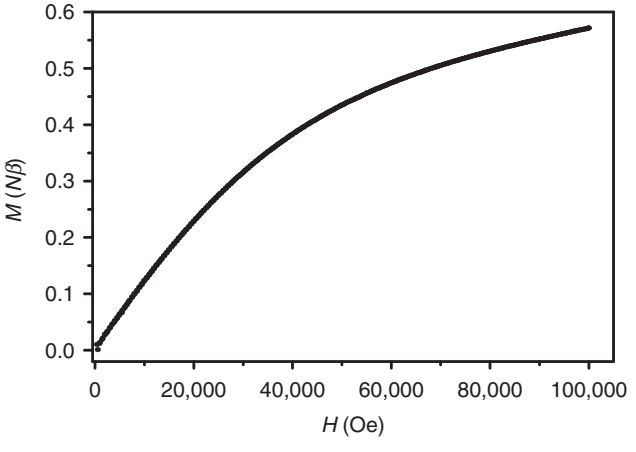


Figure 7. Magnetization *vs.* field (Oe) measurements for **3** (at 3 K).

which may be associated with magnetic ground state, low-lying magnetic excited states, or paramagnetic impurities.

**Complex 3.** The complex has $\chi_M T$ of 1.11 cm$^3$ mol$^{-1}$ K (2.97 $\mu_B$) at room temperature (figure 6). On decreasing the temperature from 300 to 2 K, a steady decrease is observed in the value of $\chi_M T$, which suggests intrachain antiferromagnetic interaction. The value of $\chi_M T$ at 2 K is 0.19 cm$^3$ mol$^{-1}$ K (1.22 $\mu_B$), which is a signature of antiferromagnetic coupling between the $Cu^{II}$ ions. A satisfactory fit was obtained with $J_{12} = -1.76\,cm^{-1}$, $g_{Cu} = 2.156$, TIP $= 5 \times 10^{-6}$ cm$^3$ mol$^{-1}$[60], $\theta = -0.35$ K, and PI $= 0.43\%$. The magnetization *versus* magnetic field isotherm at 3 K (figure 7) shows a monotonic increase that recalls a Brillouin-like function characteristic of the paramagnetic state.

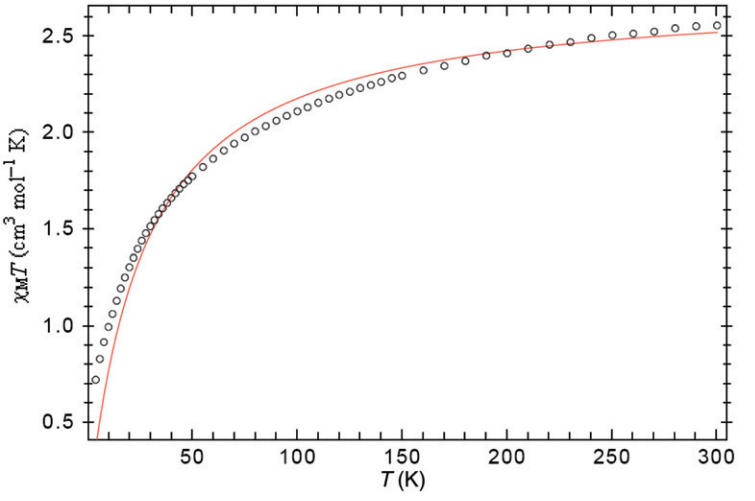


Figure 8. $\chi_M T$ *vs.* $T$ plot for **4** at 1 T: circle (experimental) and red line (calculated) with the parameters reported in the text.

Saturation of the magnetization is not reached even at 10 T and a maximum value of $0.57\,N\beta$ is obtained at 3 K. Assuming that the total magnetization comes from the contribution of two $Cu^{II}$ ($S=1$, $g_{eff}=2.156$), saturation magnetization should attain a value of $2.15\,N\beta$. The lack of saturation magnetization suggests antiferromagnetic coupling. The intrachain antiferromagnetic coupling between the spins on two metal ions occurs *via* the highly conjugated bridging ligand.

**Complex 4.** The $\chi_M T$ value ($2.71\,cm^3\,mol^{-1}\,K$, $4.65\,\mu_B$) at 300 K for the $Cu^{II}$–$Co^{II}$ complex (figure 8) is higher than the expected value of $2.25\,cm^3\,mol^{-1}\,K$ ($4.24\,\mu_B$) for non-interacting ions ($S_{Cu}=½$, $S_{Co}=3/2$; $g_{Cu}=g_{Co}=2$). This is attributed to unquenched orbital contributions (typical of the $^4T_{1g}$ ground state of octahedral $Co^{II}$ complexes [61] and $Cu^{II}$ ion). The $\chi_M T$ decreases on lowering the temperature to 2 K, characteristic of antiferromagnetic coupling between metal ions. A satisfactory fit is obtained with $J_{12}=-3.01\,cm^{-1}$, $g_{Co}=2.287$, $g_{Cu}=1.961$, $TIP=10\times10^{-6}\,cm^3\,mol^{-1}$ [62], $\theta=-0.85$ K, and PI = 0.71%.

**Complex 5.** The $\chi_M T$ (figure 9) value at 300 K is $2.07\,cm^3\,mol^{-1}\,K$ ($4.07\,\mu_B$), higher than the expected value of $1.37\,cm^3\,mol^{-1}\,K$ ($3.32\,\mu_B$) for the magnetically non-coupled $Cu^{II}$–$Ni^{II}$ ions ($S_{Cu}=½$, $S_{Ni}=1$; $g_{Cu}=g_{Ni}=2$). This is due to the significant orbital contributions from octahedrally coordinated $Ni^{II}$ and $Cu^{II}$. A monotonic decrease in $\chi_M T$ from 300 to 2 K attaining $0.37\,cm^3\,mol^{-1}\,K$ ($1.7244\,\mu_B$) at 2 K is observed. A satisfactory fit was obtained with $J_{12}=-1.96\,cm^{-1}$, $g_{Cu}=1.927$, $g_{Ni}=2.041$, $TIP=6\times10^{-6}\,cm^3\,mol^{-1}$, $\theta=-0.62$ K and PI = 0.96%. The decrease in $\chi_M T$ and negative $\theta$ are indicative of antiferromagnetic interaction. The lack of saturation in the magnetization *versus* magnetic field isotherm at 3 K is direct evidence of antiferromagnetic coupling. The saturation of the magnetization is not reached even at 10 T (Supplementary material, figure S6). A maximum value of $1.34\,N\beta$ is obtained at 3 K, which is almost half of the value ($3.00\,N\beta$) expected for $Cu^{II}$ ($S=½$, $g_{eff}=1.927$) and $Ni^{II}$ ($S=1$, $g_{eff}=2.041$).

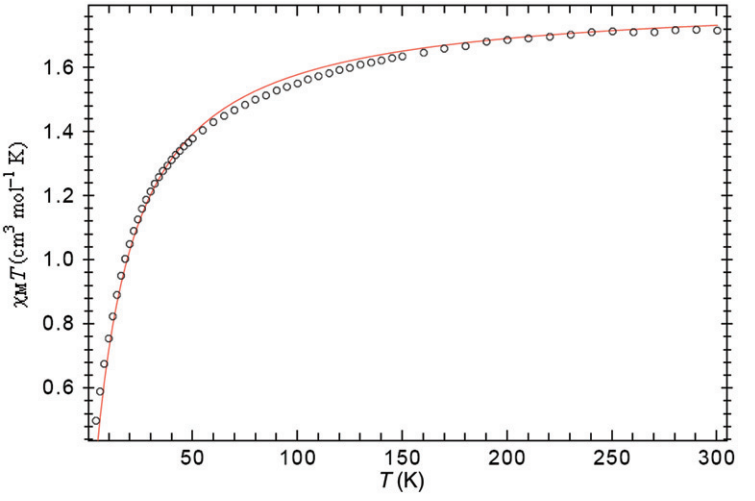


Figure 9. $\chi_M T$ *vs.* $T$ plot for **5** at 1 T: circle (experimental) and red line (calculated) with the parameters reported in the text.

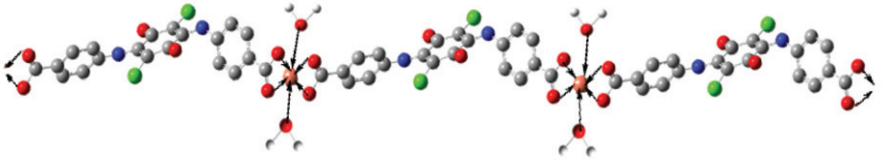

Figure 10. Schematic representation of $M^{II}M'^{II}L_2(H_2O)_4$ [$M^{II}$, $M'^{II}$ = Mn (**1**), Ni (**2**), Cu (**3**) and $M^{II}$ = Cu, $M'^{II}$ = Co (**4**), Ni (**5**)].

## 4. Conclusion

Some new homo- and hetero-bimetallic molecular assemblies, $M^{II}M'^{II}L_2(H_2O)_4$ (where $M^{II}$, $M'^{II}$ = Mn, Ni, Cu, and $M^{II}$ = Cu and $M'^{II}$ = Co, Ni) have been prepared and characterized. The 2,5-bis(4-carboxyphenylamino)-3,6-dichloro-1,4-benzoquinone bridges two metal ions in uninegative bidentate chelating fashion. Octahedral coordination around the 3d-metal ions is inferred from electronic spectra. The triclinic primitive unit lattice for the ligand as well as for the metal complexes has been deduced from powder XRD. All the coordination polymers display a 1-D chain with triclinic primitive crystal lattice. In the complexes, although the two metal centers are separated by the large ligand, an antiferromagnetic interaction ($J = -1.01$ to $-3.01\,cm^{-1}$) has been observed, due to the major role of the highly conjugated $\pi$-delocalized ligand in propagating the magnetic coupling. This is commensurate with the magnetic interaction ($J = -3.2\,cm^{-1}$) reported by Hendrickson *et al.* [47] for $[Cu_2(trenz)_2(BZD)](NO_3)_4$, where the two metal centers are separated by more than 12 Å. The stronger antiferromagnetic coupling ($J = -12.65\,cm^{-1}$) in $[Ni_2(2,2\text{-bipy})_2(pdc)(N_3)(H_2O)_2]\cdot 2H_2O$ reported by Xie *et al.* [63] is due to small Ni–Ni separation (4.472 Å). Based on the above studies structure deduced for the metal complex is shown in figure 10.

**Acknowledgments**

The authors thank the Head, Department of Chemistry, Banaras Hindu University, Varanasi, for providing laboratory facilities. The authors are grateful to Mr Suryanarayan Das and Mr Kranti Kumar Sharma for their help in the magnetic data recording. Thanks are also due to I.T.(B.H.U.) for powder X-ray data, CDRI, Lucknow for FAB-MS, SAIF IIT, Mumbai for TGA analysis, Mr Satish Tiwari for CHN analyses and Mr V.N. Pandey for IR and electronic spectra recording. One of the authors (KRR) thanks BHU for research scholarship.



**References**

[1] C. Janiak. *Dalton Trans*., 2781 (2003).
[2] S.L. James. *Chem. Soc. Rev*., **32**, 276 (2003).
[3] D. Maspoch, D. Ruiz-Molina, J. Veciana. *J. Mater. Chem*., **14**, 2713 (2004).
[4] S.R. Batten, K.S. Murray. *Coord. Chem. Rev*., **246**, 103 (2003).
[5] S. Subramanian, M.J. Zaworotko. *Angew. Chem. Int. Ed*., **34**, 2127 (1995).
[6] P. Losier, M.J. Zaworotko. *Angew. Chem. Int. Ed*., **35**, 2779 (1996).
[7] M. Fujita, J. Yazaki, K. Ogura. *Tetrahedron Lett*., **32**, 5589 (1991).
[8] R.H. Groeneman, L.R. MacGillivray, J.L. Atwood. *Inorg. Chem*., **38**, 208 (1999).
[9] C. Oldham. In *Comprehensive Coordination Chemistry*, G. Wilkinson, R.D. Gillard, J.A. McCleverty (Eds.), Vol. 2, p. 435, Pergamon Press, Oxford, UK (1987).
[10] M. Soler, W. Wernsdorfer, K. Folting, M. Pink, G. Christou. *J. Am. Chem. Soc*., **126**, 2156 (2004).
[11] N. Aliaga-Alcalde, R.S. Edwards, S.O. Hill, W. Wernsdorfer, K. Folting, G. Christou. *J. Am. Chem. Soc*., **126**, 12503 (2004).
[12] Y. Niu, Y. Song, H. Hou, Y. Zhu. *Inorg. Chem*., **44**, 2553 (2005).
[13] L. Tian, W. Zhang, B. Yang, P. Lu, M. Zhang, D. Lu, Y. Ma, J. Shen. *J. Phys. Chem. B*, **109**, 6944 (2005).
[14] S. Bordiga, C. Lamberti, G. Ricchiardi, L. Regli, F. Bonino, A. Damin, K.P. Lillerud, M. Bjorgen, A. Zecchina. *Chem. Commun*., 2300 (2004).
[15] E. Colacio, J.P. Costes, J.M. Domínguez-Vera, I.B. Maimoun, J. Suárez-Varela. *Chem. Commun*., 534 (2005).
[16] Q. Yue, J. Yang, G.H. Li, G.D. Li, W. Xu, J.S. Chen, S.N. Wang. *Inorg. Chem*., **44**, 5241 (2005).
[17] O. Kahn. *Molecular Magnetism*, VCH, New York (1993).
[18] R.D. Willet, D. Gatteschi, O. Kahn. *Magneto-Structural Correlation in Exchange Coupled Systems*, NATO ATI Series C140, Reidel, Dordrecht, The Netherlands (1985).
[19] D. Gatteschi, O. Kahn, J. Miller (Eds.). *Molecular Magnetic Materials*, NATO ASI Series E198, Kluwer, Dordrecht, The Netherlands (1991).
[20] E. Coronado, P. Delhaes, D. Gatteschi, J. Miller (Eds.). *Molecular Magnetism: From Molecular Assemblies to the Devices*, NATO ASI Series E321, Kluwer, Dordrecht, The Netherlands (1996).
[21] F. Prins, E. Pasca, L.J. de Jongh, H. Kooijman, A.L. Spek, S. Tanase. *Angew. Chem., Int. Ed*., **46**, 6081 (2007).
[22] S. Tanase, J. Reedijk. *Coord. Chem. Rev*., **250**, 2501 (2006).
[23] E. Chelebaeva, J. Larionova, Y. Guari, R.A. Sá Ferreira, L.D. Carlos, F.A.A. Paz, A. Trifonov, C. Guérin. *Inorg. Chem*., **47**, 775 (2008).
[24] Y.Z. Zhang, Z.M. Wang, S. Gao. *Inorg. Chem*., **45**, 5447 (2006).
[25] Z.-X. Wang, X.-L. Li, B.-L. Liu, H. Tokoro, P. Zhang, Y. Song, S.-I. Ohkoshi, K. Hashimoto, X.-Z. You. *Dalton Trans*., 2103 (2008).
[26] P. Jensen, D.J. Price, S.R. Batten, B. Moubaraki, K.S. Murray. *Chem. Eur. J*., **6**, 3186 (2000).
[27] R. Pellaux, H.W. Schmalle, R. Huber, P. Fischer, T. Hauss, B. Ouladdiaf, S. Decurtins. *Inorg. Chem*., **36**, 2301 (1997).
[28] C.H. Ge, A.L. Cui, Z.H. Ni, Y.B. Jiang, L.F. Zhang, J. Ribas, H.Z. Kou. *Inorg. Chem*., **45**, 4883 (2006).
[29] J.M. Domínguez-Vera, J. Suárez-Varela, I.B. Maimoun, E. Colacio. *Eur. J. Inorg. Chem*., 1907 (2005).
[30] T.K. Karmakar, S.K. Chandra, J. Ribas, G. Mostafa, T.H. Lu, B.K. Ghosh. *Chem. Commun*., 2364 (2002).
[31] L. Zhang, L.F. Tang, Z.H. Wang, M. Du, M. Julve, F. Lloret, J.T. Wang. *Inorg. Chem*., **40**, 3619 (2001).

[32] C.D. Ene, F. Tuna, O. Fabelo, C. Ruiz-Pérez, A.M. Madalan, H.W. Roesky, M. Andruh. *Polyhedron*, **27**, 574 (2008).
[33] D. Braga, F. Grepioni, A.G. Orpen. *Crystal Engineering: From Molecules and Crystals to Materials*, NATO Science Series, Series C, p. 538, Kluwer Academic, Dordrecht (1999).
[34] S.C. Manna, E. Zangrando, A. Bencini, C. Benelli, N.R. Chaudhuri. *Inorg. Chem.*, **45**, 9114 (2006).
[35] S.C. Manna, E. Zangrando, J. Ribas, N.R. Chaudhuri. *Dalton Trans.*, 1383 (2007).
[36] S.C. Manna, E. Zangrando, M.G.B. Drew, J. Ribas, N.R. Chaudhuri. *Eur. J. Inorg. Chem.*, 481 (2006).
[37] L. Applegarth, A.E. Goeta, J.W. Steed. *Chem. Commun.*, 2405 (2005).
[38] S.C. Manna, J. Ribas, E. Zangrando, N.R. Chaudhuri. *Inorg. Chim. Acta*, **360**, 2589 (2007).
[39] D. Sun, Y. Ke, T.M. Mattox, B.A. Ooro, H.-C. Zhou. *Chem. Commun.*, 5447 (2005).
[40] S.R. Seidel, P.J. Stang. *Acc. Chem. Res.*, **35**, 972 (2002).
[41] A.K. Ghosh, D. Ghoshal, E. Zangrando, J. Ribas, N.R. Chaudhuri. *Dalton Trans.*, 1554 (2006).
[42] X.-Y. Wang, H.-Y. Wei, Z.-M. Wang, Z.-D. Chen, S. Gao. *Inorg. Chem.*, **44**, 572 (2005).
[43] R.A. Morton. *Biochemistry of Quinones*, Academic Press, New York (1965).
[44] S. Patai. *The Chemistry of the Quinoid Compounds*, Wiley, Chichester (1974).
[45] B.L. Trumpower. *Functions of Quinones in Energy Converting Systems*, Academic Press, New York (1982).
[46] J.P. Klinman, D. Mu. *Annu. Rev. Biochem.*, **63**, 299 (1994).
[47] T.R. Felthouse, E.N. Duesler, A.T. Christenson, D.N. Hendrickson. *Inorg. Chem.*, **18**, 245 (1979).
[48] E. König. *Magnetic Properties of Coordination and Organometallic Transition Metal Compounds*, Springer, Berlin (1966).
[49] Available online at: http://ewww.mpi-muelheim.mpg.de/bac/logins/bill/julX_en.php
[50] M. Kılıç, Z. Çınar. *J. Mol. Struct: Theochem.*, **53**, 808 (2007).
[51] M.J. Frisch, G.W. Trucks, H.B. Schlegel, G.E. Scuseria, M.A. Robb, J.R. Cheeseman, J.A. Montgomery Jr, T. Vreven, K.N. Kudin, J.C. Burant, J.M. Millam, S.S. Iyengar, J. Tomasi, V. Barone, B. Mennucci, M. Cossi, G. Scalmani, N. Rega, G.A. Petersson, H. Nakatsuji, M. Hada, M. Ehara, K. Toyota, R. Fukuda, J. Hasegawa, M. Ishida, T. Nakajima, Y. Honda, O. Kitao, H. Nakai, M. Klene, X. Li, J.E. Knox, H.P. Hratchian, J.B. Cross, V. Bakken, C. Adamo, J. Jaramillo, R. Gomperts, R.E. Stratmann, O. Yazyev, A.J. Austin, R. Cammi, C. Pomelli, J.W. Ochterski, P.Y. Ayala, K. Morokuma, G.A. Voth, P. Salvador, J.J. Dannenberg, V.G. Zakrzewski, S. Dapprich, A.D. Daniels, M.C. Strain, O. Farkas, D.K. Malick, A.D. Rabuck, K. Raghavachari, J.B. Foresman, J.V. Ortiz, Q. Cui, A.G. Baboul, S. Clifford, J. Cioslowski, B.B. Stefanov, G. Liu, A. Liashenko, P. Piskorz, I. Komaromi, R.L. Martin, D.J. Fox, T. Keith, M.A. Al-Laham, C.Y. Peng, A. Nanayakkara, M. Challacombe, P.M.W. Gill, B. Johnson, W. Chen, M.W. Wong, C. Gonzalez, J.A. Pople. *Gaussian 03, Revision C.02*, Gaussian, Inc., Wallingford, CT (2004).
[52] X. Wang, L. Andrews. *J. Phys. Chem. A*, **110**, 10035 (2006).
[53] K. Nakamoto. *Infrared and Raman Spectra of Inorganic and Coordination Compounds*, 4th Edn, p. 232, Wiley Interscience – John Wiley & Sons, New York (1986).
[54] A. Tavmana, I. Bozb, A.S. Birteksözc, A. Cinarli. *J. Coord. Chem.*, **63**, 1398 (2010).
[55] A.M. Khedra, D.F. Draza. *J. Coord. Chem.*, **63**, 1418 (2010).
[56] L.B. Azaroff, M.J. Burger. *The Powder Method in X-ray Crystallography*, McGraw Hill, New York (1958).
[57] G.-G. Gao, L. Xu, W.-J. Wang, X.-S. Qu, H. Liu, Y.-Y. Yang. *Inorg. Chem.*, **47**, 2325 (2008).
[58] C.-I. Yang, W. Wernsdorfer, Y.-J. Tsai, G. Chung, T.-S. Kuo, G.-H. Lee, M. Shieh, H.-L. Tsai. *Inorg. Chem.*, **47**, 1925 (2008).
[59] F.-M. Nie, S. Demeshko, S. Fuchs, S. Dechert, T. Pruschke, F. Meyer. *Dalton Trans.*, 3971 (2008).
[60] G. Yucesan, V. Golub, C.J. O'Connor, J. Zubieta. *Dalton Trans.*, 2241 (2005).
[61] F.E. Mabbs, D.J. Machin. *Magnetism and Transition Metal Complexes*, Chapman and Hall, London (1973).
[62] K.I. Pokhodnya, M. Bonner, A.G. DiPasquale, A.L. Rheingold, J.-H. Her, P.W. Stephens, J.-W. Park, B.S. Kennon, A.M. Arif, J.S. Miller. *Inorg. Chem.*, **46**, 2471 (2007).
[63] C.-Z. Xie, Y.-Z. Liu, Q.-j. Su, Y. Ouyang, J.-Y. Xu. *J. Coord. Chem.*, **63**, 801 (2010).